CARRIER TRANSPORT PROPERTIES, SPECTRAL PHOTORESPONSE, AND BANDGAP STRUCTURE FEATURES IN pnn^+-GaAs WITH PATTERNED NANOSCALE As_2O_3–GaAs INTERFACE

T.YA. GORBACH, L.A. MATVEEVA, P.S. SMERTENKO, G.A. SUKACH

V. Lashkarev Institute of Semiconductor Physics, Nat. Acad. Sci. of Ukraine
(45, Nauky Prosp., Kyiv 03680, Ukraine; e-mail: smertenko@isp.kiev.ua)

UDC 621.315.592

An advanced patterned As_2O_3—pnn^+-GaAs structure has been examined by the current-voltage characteristics (IVC), photoresponse (PR) spectral measurements, SEM image study, X-ray analysis, and electroreflectance (ER) spectroscopy for a novel optical design and the observation of transport phenomena. The patterned semiconducting medium has been developed simultaneously with the arsenolite oxide phase of As_2O_3 by anisotropic chemical etching (ACE) in a $(10\div15)N$ HNO_3 solution at the p-type top surface of the pnn^+-GaAs structure. This medium is found to consist of the skeleton-dendritic morphology with a size of about 5–10 μm covered by chemisorbed nanoscale As_2O_3 and non-stoichiometric layers with Ga vacancies and free As at the interface As_2O_3–GaAs. It is shown that, under favourable patterning conditions, the inversion layer near a surface with triangular potential well of a variable width from 14 to 25 nm has been formed. In this case, the negative differential resistance (NDR) region with oscillation behavior and the peak-to-valley ratio (PVR) from 10 to 100, which is typical of a quantized structure, has been observed on dark forward (fw) I–V characteristic (IVC). Spectral data have shown the improving of the short-wavelength response as the long-wavelength one. The effect of a patterning regime on photovoltaic (PV) parameters is found as well. For a higher reverse (rv) voltage, the increasing of PR by up to 4 orders has been realized due to the avalanche multiplication. The photoresponse detection beyond the normal absorption edge of GaAs has been demonstrated because of the Franz—Keldysh effect.

A possible model of evolution of the skeleton-dendritic multilayer patterned As_2O_3—pnn^+-GaAs structure during ACE is proposed. The carrier transport mechanism and bandgap structure features have been discussed.

1. Introduction

Within two past decades, there appear a number of spectacular advances in the research of semiconductors (IV group, III–V compounds, etc.) through the band gap engineering and limited dimensional structures (quantum confinement), as well as in the construction of novel device structures using the technological progress in their fabrication (modulation doped technologies, lattice-matched epitaxy, modified patterned design of surfaces and interfaces, etc.). Among the techniques that have been widely used for the achievement of unique physical properties are the molecular beam and liquid-phase epitaxy (MBE, LPE) and the chemical and metal-organic chemical vapour deposition (CVD, MOCVD) [1–3]. The wet anisotropic chemical and electrochemical etchings (ACE, AECE) are also important processing procedures for materials science and physics of structures on nanometer scale, changes in their stoichiometry, and ease oxide phase formation [4–7].

This article presents some advances in the classic pnn^+GaAs structure chemically processed to patterned multilayer including the vacancy layer, thin oxide layer and patterned oxide – semiconductor interface. Investigation will focus on useful anomalous properties and examine their potential for irradiance monitoring.

2. Experimental

The study was undertaken with pnn^+-test structures on Te-doped n^+-GaAs{100} substrate with a concentration of 8×10^{18} – 2×10^{19} cm^{-3} and a thickness of about 300 μm. The 10–15 μm Si-doped (n-type) and a 10–15 μm thick Zn-doped (p-type) epilayers with a carrier concentration of about 8×10^{16} – 1×10^{17} cm^{-3} were deposited by the CVD process.

All pattern preparation on a front p-type surface was carried out in a 10–15N HNO_3 solution during 2.0, 3.0, 5.0, and 10.0 s ($t_{1\mathrm{ACE}}$) at room temperature. In the previous experiments [4, 8], it was shown that the patterned interface As_2O_3–GaAs may be formed simultaneously with the patterned morphology. To remove As_2O_3, the test structures were loaded in a 5% KOH solution at 353 K for 5.0 and 20.0 s ($t_{2\mathrm{ACE}}$).

The modified morphology and stoichiometry were studied by SEM (S-806 Hitachi) and a Superprobe-733 (JEOL), respectively. The static forward and reverse I–V characteristics of In—(As_2O_3)—pnn^+-GaAs—In structure were measured by an automatized 14-TKS-100 tester (Russia) in dark and under illumination. A Xenon lamp was used as the radiation source with intensity equivalent to the 0.03 Sun's one. Either a quad-ring or a mesa was applied. The sample area was 5×5 cm^2.

The PR spectra were measured in the spectral range between 300 and 1100 nm with the use of the standard equipment in the short-circuit current regime and under the photodiode mode. The photocurrent gain $G(V)$ was determined as a multiplied photocurrent $I_{M\mathrm{ph}}$ divided by the photocurrent at a low voltage where no current multiplication takes place.

The IVC differential slope [9] and the concept of quantum confinement [1, 10] were used for the analysis of a carrier transport mechanism.

To probe the bandgap structure, the electroreflectance (ER) spectroscopy was carried out in GaAs (or As_2O_3—GaAs) – 0.1 N KCl system by the classical modulation technique [11] in the range 2.4–3.4 eV in the low-field mode at 273 K. As a diagnostic indicator, the transition energy E_1 at a critical point of the Brillouin zone in $\langle 111\rangle$, the spin-orbit splitting energy Δ_1, and the phenomenological broadening parameters Γ_1 and $\Gamma_{1+\Delta1}$ were used. In our case, we used the high absorbed illumination $\alpha\approx(3\div7)\times10^5$ cm^{-1} to study both the ultra thin surface layer and the interfacial As_2O_3—pnn^+-GaAs one on a nanoscopic scale ($\leq$ 30 nm).

3. Results and Discussion

3.1. Patterned morphology

Figure 1,*a,b,c* illustrates several of the possible morphologies after ACE. Figure 1,*d* is the image of a fragment of the GaAs patterned surface after the chemical oxidation (top) during ACE and the oxide removing (bottom). Figure 1,*e* presents the cross-sectional view of – pnn^+-GaAs after ACE. The SEM observation shows the presence of the diversity of geometries such as a classical pyramid and a non-classical (quasipyramid) one with additional small (less than 50 nm in size) pyramids, which are full of holes, on the facets, and the skeleton and dendrite forms.

The pyramid facets, dendrite branches, and another patterned formations may exhibit both the low-index {111} surface and high-Miller-index surfaces including {211}, {311}, etc. [12].

While modified GaAs is exposed in HNO_3 at room temperature, the surface is covered by oxygen ions. If the exposure time is increased, the crystalline arsenic oxide As_2O_3 (arsenolite), being the state previously observed in both reflectance and transmittance measurements [8], is grown on the patterned GaAs surface. Arsenolite is a cubic crystal with a energy bandgap near 5 eV. The development of the As_2O_3 morphology can be described using the hypothesis of a three-step anisotropic chemical reaction.

For example, for the quasipyramid and skeleton-dendritic formations, the first step deals with the missing of Ga atoms and the production of Ga vacancies near the surface (a few atomic layers). This process induces the vacancy energy level $E_v+(0.2\div0.4)$ eV. By forming a Ga vacancy, the surface bonds are broken, and As dangling bonds are created. This process can be described by the creation of the energy level $E_c-(0.45\div0.2)$ eV. Arsenic acts as an apparent electron donor resulting to a decrease of the p-type conductivity in the thin (atomic) layer. Such a "doping" by the pentavalent anion is accompanied by forming the depleted region at the surface. As a result, the bands are bent. The arsenic surface state will pin the Fermi level.

The second step is characterized by the oxygen chemisorption. At first, the adsorpted oxygen is covered the surface by O_2^- ions, then oxygen builds the covalent bond with As. The bond length of O—As is 0.18 nm. Further, oxygen is incorporated in a vacancy and the V_{Ga}+O_{As} surface configuration is constructed [4]. This complex may create the deep level $E_c-(0.65\div0.76)$ eV or $E_c-0.4$ eV. In this case, the surface region is inverted to an n-type layer and can modify the Fermi level pinning. It is entirely possible that two last steps occur simultaneously.

In the third step, there is a strong interaction between the surface and an oxygen atom with the formation of a new phase of As_2O_3. During the process of oxide thickening, it is reasonable to assume that the exhaustion of arsenic may take place.

Therefore, depending on the etching and oxidation stages, the surface and interfacial layers can be

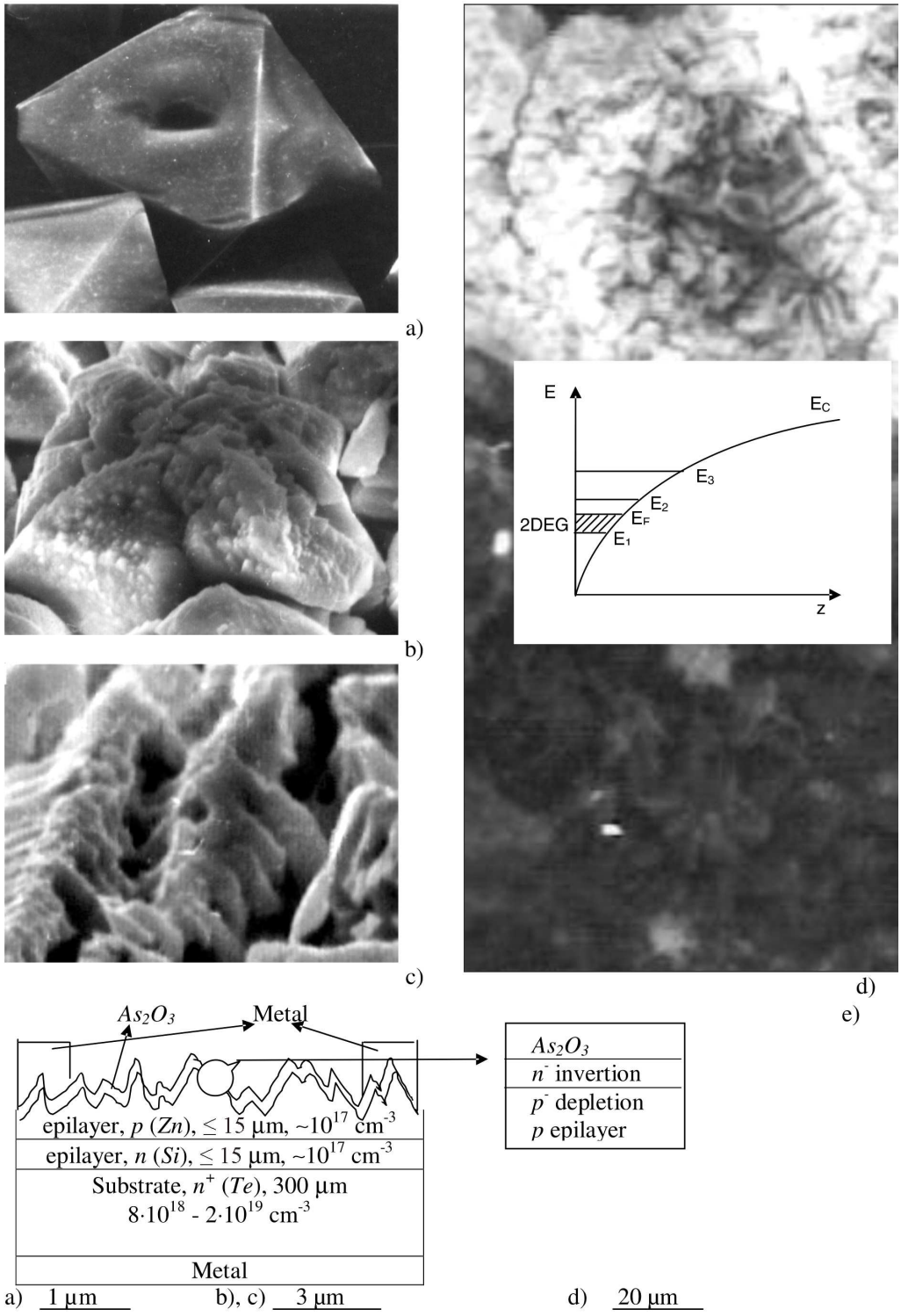

Fig. 1. SEM image (*a–d*) of GaAs and cross-sectional view (*e*) of pnn^+-GaAs with patterned morphologies: *a* – quasipyramid, *b* – skeleton form, *c* – dendrite branches, *d* – fragment of patterned As_2O_3—GaAs (top) and GaAs after the oxide removing (bottom), *e* – cross-sectional view of pnn^+-GaAs after ACE. In the insert to Fig. 1,*d* – schematic drawing of band diagram at interface As_2O_3—GaAs. On a detail in Fig. 1*e* – fragment of As_2O_3—*p*-GaAs interface

heterogeneously nonstoichiometric due to the crystallographic mixture of patterned figures associated with various facet orientations.

Using the ratio of X-ray intensities $R = (I_{\mathrm{Ga}} - k_\alpha)/(I_{\mathrm{As}} - k_\alpha)$ in X-ray analysis as an indicator of the chemical decomposition, it was shown that $2.2 < R \leq 1.6$ for the nonpatterned surface; $0.65<R<0.85$ for the quasipyramid with oxygen adsorption, and $0.12<R<0.65$ for the skeleton-dendritic form, when the oxide phase is formed. Although the absolute accuracy of such an analysis may be in doubt, this is useful as a qualitative guide.

When the bands are strongly bent, the potential triangular well formed by As_2O_3—GaAs surface can be sufficiently narrow, and carriers are confined to a region close to the interface. The motion of carriers in the potential well is constrained in the direction perpendicular to the surface, i.e. it is two-dimensional in nature. If the well thickness is about the electron de Broglie wavelength, the energy level quantization occurs. In principle under these conditions, it is possible to change the transport mechanisms in pnn^+-GaAs structure and to get the novel properties and characteristics. The workable approximation of a potential triangular well with three levels is presented in the insert in Fig. 1,*d*.

3.2. I–V characteristics

The current vs. voltage behaviors before and after patterned steps are presented in Fig. 2. As seen from Fig. 2,*a,b*, the fw and rv IVCs of the nonpatterned (flat) structure are asymmetric and enough far from the ideal diode one. At low voltages, the dark fw IVC has $I \sim V^2$ region. At a higher bias (3–9 V), has exponential region with a large ideality factor of about 25. This undesirable high injection mechanism can be due, very likely, to the leakage current at the surface periphery of the structure, particularly under a rv bias ($I \sim V^4$).

No change or only a slight change is observed in IVC after the treatment in HNO_3 for 2 s in comparison with the nonpatterned case.

In contrast, for 2 s $\leq t_{1\mathrm{ACE}} \leq$ 5 s, the dark IVCs have, at least, two attractive features as demonstrated in Fig. 2,*c,d*. First, after the ohmic start out at a low voltage, the fw IVCs (Fig. 2,*c*, curves *1, 1**) exhibit the NDR regions under a higher one. Increasing $t_{1\mathrm{ACE}}$ from 2 s to 5 s is accompanied both by changes in the NDR character, the PVR, the classic peak voltage position (V_{cl}), and the quantum peak one (V_{qu}). If the quasipyramid pattern is produced (Fig. 1,*a*) $V_{\mathrm{cl}} = 0.7$ V, and the region of NDR with PVR≈10 is observed (curve *1**, Fig. 2,*c*). At $t_{1\mathrm{ACE}} = 5$ s, there are the oscillatory phenomena in NDR with several PVR about 50 and 100. It seems reasonable to assume that NDRs are either due to discrete levels in the double barrier surface structure (well) for the tunnelling of carriers, which open up under a definite bias or even due to a few QW (superlattice) structure. The assumption of the superlattice presence does not lead to its easy interpretation. At least three remarks should be made:

(i) Due to the coexistence of the diversity of atomic and electronic structures of the start low index {100} surface and high-Miller-index ones, for example, {211}, {311}, {511}, etc. in the pattern morphology [12], it is possible to obtain the superlattice organization by the surface orientation.

(ii) On the other hand, the ACE treatment can perturb the surface and interface compositions, and this situation may yield the modulated doping or a variable gap superlattice.

(iii) In addition, the numerical results were obtained in the infinitely deep rectangular well (superlattice) approximation and have only qualitative sense for our triangular well.

Then the energy of levels E_n can be self-consistently calculated using the superlattice approximation. According to [1, 10], the superlattice period d is given by the formula $d = hl/2\pi eV_{\mathrm{cl}}\tau$, where h is Planck's constant, e is the electron charge, l is the active length between the contacts, and τ is the relaxation time. For curves *1* and *1** (Fig. 2,*c*) $V_{\mathrm{cl}} = 0.3$ V and $V^*_{\mathrm{cl}} = 0.7$ V, respectively.

At higher voltages, we can see the second and third IVC peaks which can be appropriated to the resonance tunnelling between energy levels in the well or in neighbour wells, the so-called quantum peaks. For these peaks, $E_n = edV_{\mathrm{qu}}/l$. Introducing $d/l = h/2\pi eV_{\mathrm{cl}}\tau$, we obtain E_n as $E_n = h/2\pi\tau \times V_{\mathrm{qu}}/V_{\mathrm{cl}}$. Then, in the assumption $\tau \sim 10^{-13}$ s [10], for curve *1*, Fig. 2,*c* with $V_{\mathrm{qu1}} = 3$ V and $V_{\mathrm{qu2}} = 10$ V, we get $E_1 = 0.066$ eV and $E_2 = 0.22$ eV, respectively. For curve *1**, Fig. 2,*c*, with the peak at 5 V, we get $E_1 = 0.047$ eV. Moreover, it should be noted that the advantage of the fw IVC is the high value $I_{\mathrm{ill}}/I_d \approx 1 \times 10^4$, which is important for optical switches (for example, Fig. 2,*c*, curves *1, 2*, the applied voltage $V = 5$ V).

Second, the rv IVC displays the good dark current saturation and the breakdown voltage (V_B) increase. The breakdown is abrupt and uniform. The multiple kinks and the on-off switching sections in IVC are absent. This is the important feature for the photosensi-

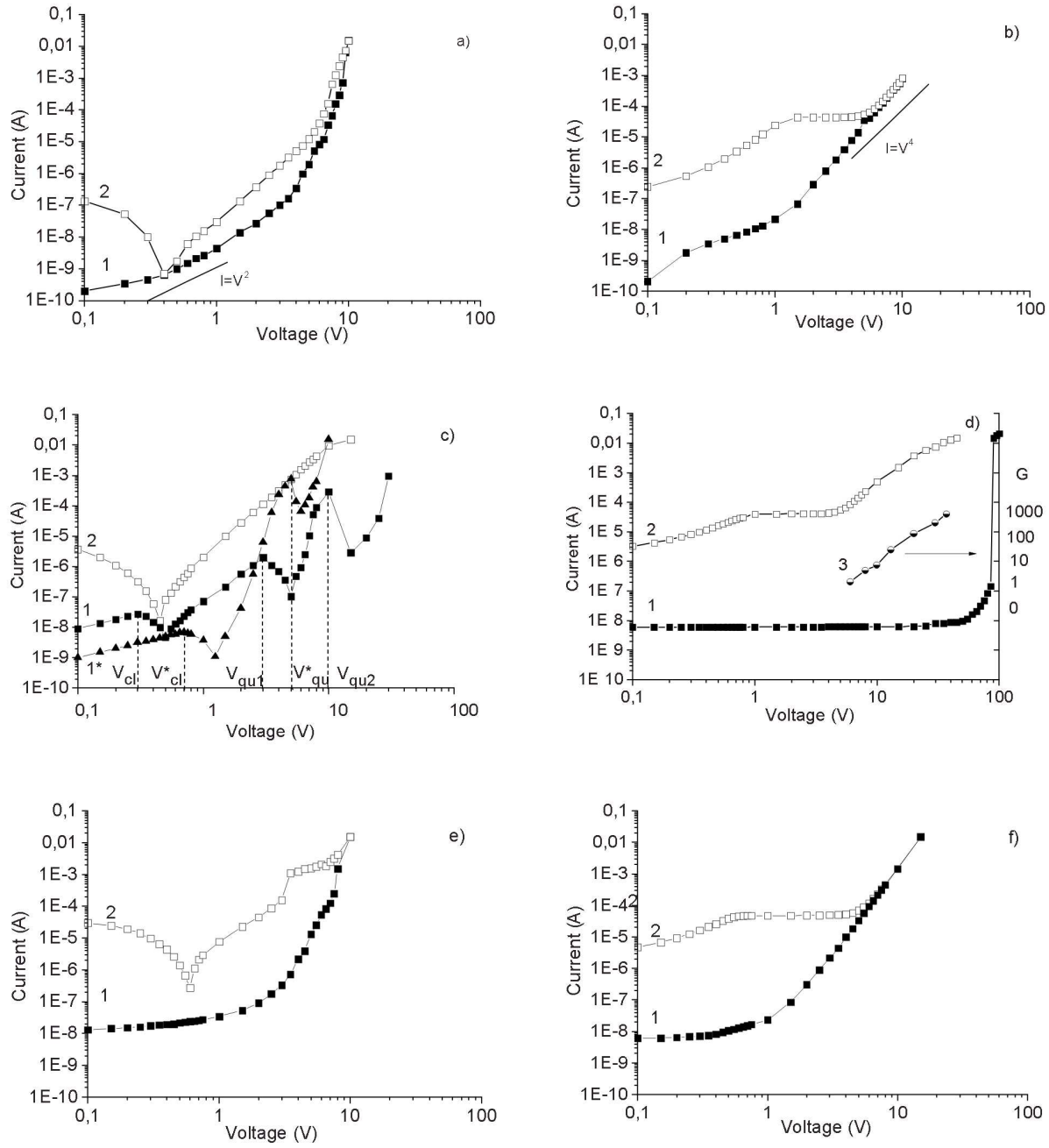

Fig. 2. IVC forward (*a, c, e*) and reverse (*b, d, f*) characteristics of pnn^+-structures: *a, b* – nonpatterned; *c, d* – patterned As_2O_3—GaAs ($t_{1ACE} = 5$ s); *e, f* – patterned GaAs after removing As_2O_3 during $t_{2ACE} = 5$ s. Curves *1, 2* were obtained in dark and under illumination, respectively. Curve *1** represents the dark IVC after $t_{1ACE} = 3$ s. V_{cl} and V_{qu} are the classical and quantum peak voltage positions. Curve *3* shows the dependence of the avalanche gain versus voltage

tivity enhancement by means of the internal amplification. Under the illumination as the bias is increased to 1 V, the rv current increases due to the better carrier collection, and then I_{ph} is practically constant up to 5 V. At voltages higher than 5 V, the photocurrent gain occurs. For example, under the rv bias $V = 0.25V_B$ and $V = 0.5V_B$, the $G \approx 88$ and $G \approx 400$, respectively. If the mechanism for the photocurrent

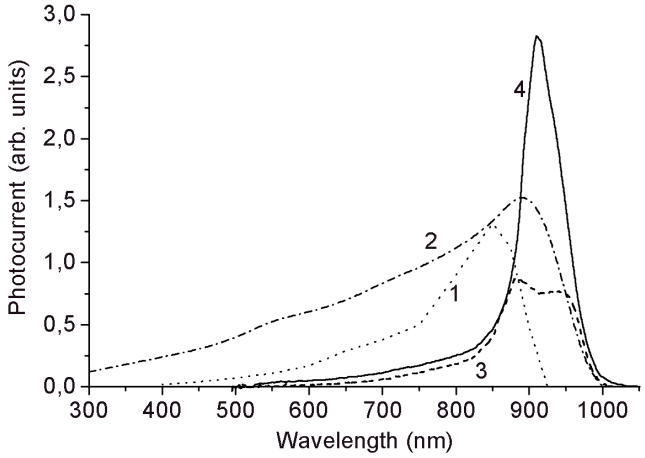

Fig. 3. Spectral response of pnn^+-GaAs structures with nonpatterned surface (*1*) and patterned one (*2*) after removing As_2O_3 in the short circuit current regime; patterned As_2O_3—GaAs (*3, 4*) without bias and under the 3-V rv bias, respectively

gain is avalanche-like, the gain in the prebreakdown region can be described by the Miller empirical relation $G = 1/\{1-(V/V_B)^m\}$ [13]. As a result, the photocurrent gain dependence on the rv bias is presented in Fig. 2,*d* (curve 3), and a plot of $G(V)$ yield $m = 1.6$.

The above-mentioned features in IVCs disappear for $t_{1\mathrm{ACE}} = 10$ s or $5 \leq t_{2\mathrm{ACE}} \leq 20$ s. In the last case, it is possible to have a loss in the quantization, and no essential difference between the nonpatterned and patterned diode characteristics is observed in practice. However, as follows from Table 1, the previous structure (As_2O_3—GaAs) may not be the best structure for photovoltaics. The optimum of I_{sc} and V_{oc} values is observed for the patterned pnn^+-structure after As_2O_3 removing during 5 s (Fig. 2,*e*).

3.3. Spectral response measurement

Fig. 3 shows the wavelength dependence of the photoresponse from two pairs of pnn^+-structures. The first pair are a nonpatterned GaAs (curve *1*) and a patterned one (curve *2*) after $t_{1\mathrm{ACE}} = 5$ s, $t_{2\mathrm{ACE}} = 5$ s. The second pair presents the binary As_2O_3—GaAs (5 s in HNO_3) structure for the zero voltage (curve *3*) and under the 3-V bias (curve *4*). Note that the IVCs of the second pair are presented in Fig. 2,*d*.

According to Fig. 3, any patterned morphology changes the PR both at the shorter and longer wavelengths. As a patterned morphology is a good light trapping (low reflection, multiple absorption) and a minimization of *p*-type thickness takes place during ACE, the short-circuit current (curve *2*) is increased in the whole spectral range. These data coincide with the table data. In addition, the PR peak position has a redshift from 860 to 880 nm, and there is a PR signal above the usual absorption edge of GaAs. But the most important changes in PR are observed from the second pair. As follows from Fig. 3 (curves *3* and *4*), these structures have more selective spectral characteristics and the further improvement of PR beyond the absorption edge. In comparison with curve *2*, curve *3*, except for the dominant peak which is the same for both structures, has a shoulder at the low-energy side caused by the Franz—Keldysh shift of the absorption edge. The last effect takes place in the As_2O_3—GaAs structure due to the internal field emerge, but it is absent in patterned GaAs, when the redshift is due mainly to the geometric factor (multiple absorption). In addition, under the 3-V rv bias, the structure (curve *4*) increases significantly the PR value, and its peak position is shifted to 912 nm. Unfortunately, no spectral measurements of such a structure were carried out at a higher bias. But, however, the results of Sections 3.2 and 3.3 allow us to discern that the As_2O_3—GaAs structure may be suitable for electroabsorption avalanche photodiode detectors [13].

3.4. Electroreflectance spectra

In this section, the data on the band transition originating from the surface and the interface on a nanoscopic scale are presented. Figure 4 depicts the ER spectra for the initial, nonpatterned (curve *1*), and patterned ($t_{1\mathrm{ACE}} = 5$ s, curve *2*) surfaces. Table 2 illustrates the zone parameters: the E_1 energy transition, the energy of spin-orbit splitting Δ_1, and the phenomenological broadening parameter both for nonpatterned and patterned surfaces.

As follows from Fig. 4 and Table 2, the values of E_1, $E_1 + \Delta_1$, and Δ_1 were found after patterning to be close to the classical ones for GaAs [11]. In addition, a decrease of the broadening parameter energy may be caused by a good structural quality of the formation of the interface As_2O_3—GaAs. Such a feature is observed repeatedly, for example, at the SiO_2 – Si interface [6]. Moreover, there

T a b l e 1. ACE effect on photovoltaic parameters

Cell parameter	Surface type			
	Nonpatterned surface	Patterned *p*-type surface		
		$T_{1\mathrm{ACE}}$=5 s	$T_{1\mathrm{ACE}}$=5, s $T_{2\mathrm{ACE}}$=5, s	$T_{1\mathrm{ACE}}$=5, s $T_{2\mathrm{ACE}}$=20, s
I_{sc}, A	1.5×10^{-7}	5×10^{-6}	5×10^{-5}	7×10^{-7}
V_{oc},V	0.4	0.5	0.6	0.6

are other remarkable features in the ER spectrum of the patterned surface in comparison with a nonpatterned one:
(i) the inversion of the ER signal polarity;
(ii) the splitting of dominating peaks;
(iii) the formation of a fine peaked structure of the line shape which is seen most clearly on the short-energy shoulder of the ER spectrum.

These anomalous phenomena may be resulted from:
(i) the conductivity type conversion from the p- to n-type, i.e. under the formation of the As_2O_3—GaAs interface of the inversion layer and a strong electrical field in parallel to the interface;
(ii) the decrease in the dimensionality from 3D to 2D for the carrier motion in the direction perpendicular to the interface due to the formation of a quantum well (QW) with quantized levels (QLs) in the two-dimensional electron gas (2DEG) channel.

For a triangular QW, the energy positions of QLs are approximated by the formula [1]

$$E_n = \left(\frac{(h/2\pi)^2}{2m^*}\right)^{1/3} \left[\frac{3}{2}\pi e F_S \left(n + \frac{3}{4}\right)\right]^{2/3}$$

or

$$E_n = \left(\frac{(h/2\pi)^2}{2m^*}\right)^{1/3} \left[\frac{3}{2}\pi e^2 \frac{N_S}{\varepsilon_0 \varepsilon} \left(n + \frac{3}{4}\right)\right]^{2/3},$$

where m^* is the longitudinal effective electron mass for the E_1 transition, $m^* = 0.053 m_0$, m_0 is the free electron mass, F_s is a surface built in the electric field, ε_0 and ε are the dielectric permittivities of vacuum and the semiconductor, respectively, N_s is the inversion carrier concentration, and n is the quantum number (0, 1, 2, etc.).

On the other hand, for each separated subband located in a QW, the energy position of a QL may be approximated by $E_n = \frac{(h/2\pi)^2}{m^*}\left(\frac{n\pi}{L}\right)^2$ as for a rectangular QW, where L is the subband width and n is equal to 1, 2, 3, etc. in this case [1].

Thus, using the combination of both approximations and considering the existence of three subbands attributed to 3 peaks in the short-energy region of the ER spectrum, the width L of a QW, F_s, and N_s were calculated and are summarized in Table 3.

It is necessary to note that the ER measurements were located by a nanoscopic slope, and its data are most severe in comparison with the IVC data. Hereby, the object of investigations was to understand the evolution situation from pnn^+-GaAs nonpatterned structure to the As_2O_3—pnn^+-GaAs patterned one more qualitatively than quantitatively. Nevertheless, such quantitative findings as the QL position and the QL number determined both from the IVC measurements and the ER data still hold true. We note that some authors evaluated the structure of energy levels using a half value of the voltage corresponding to the NDR peak positions on IVCs [1].

T a b l e 2. ACE effect on the zone parameters of pnn^+-GaAs

Surface type	Zone parameters, eV				
	E_1	$E_1 + \Delta_1$	Δ_1	Γ_1	$\Gamma_{1+\Delta 1}$
Nonpatterned	2.969	3.161	0.192	0.119	0.104
Patterned As_2O_3—GaAs $t_{1ACE} = 5$ s	2.895	3.105	0.210	0.090	0.089

T a b l e 3. Experimental energy position of a QL and some parameters of the patterned As_2O_3—pnn^+-GaAs interface

Experimental position of QL E_n, eV	Width of QW, L, nm	E_s, V/cm^2	N_s, cm^2
0.036	14.08	2.27×10^5	1.63×10^{12}
0.064	21.11	2.31×10^5	1.66×10^{12}
0.093	25.7	2.61×10^5	1.87×10^{12}

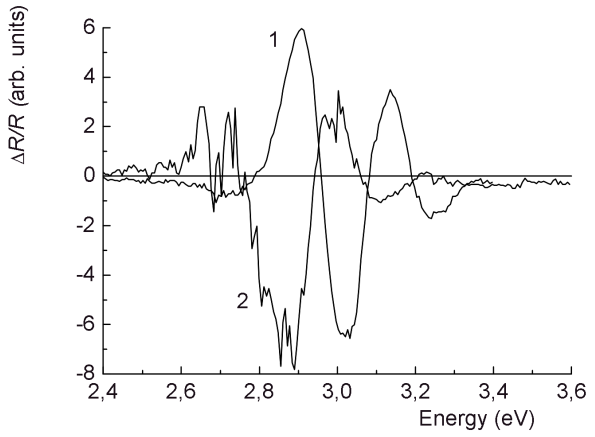

Fig. 4. ER spectra of pnn^+-GaAs structures with nonpatterned (*1*) and patterned As_2O_3—GaAs (*2*) surfaces

4. Conclusion

The ability to construct a new patterned As_2O_3—GaAs heterojunction structure from a flat classic pnn^+-GaAs structure using the wet anisotropic chemical etching has been demonstrated. A new patterned structure includes the n-inverted layer consisting of As-rich (the

As sublattice) and Ga vacancies sandwiched between patterned As_2O_3 oxide and the p-type depleted top epitaxial layer to obtain a new optical design and to control its properties. The inversion layer is presented by the triangular quantum well with a variable width from 14 to 26 nm and the 0.036-, 0.064-, and 0.093-eV positions of QLs in the QW.

The inspection of the patterned morphology, its chemical composition, the patterned interface, transport properties, photosensitivity, and zone parameters by using SEM, X-ray analysis, current-voltage characteristics, spectral response, and electroreflectance monitoring has revealed the multifunctionality of the patterned As_2O_3—pnn^+-GaAs structure:
(i) an optical bistable device under condition of the 2D carrier transport;
(ii) a potentially useful optical design with the performance of a photovoltaic cell;
(iii) an electroabsorption avalanche photodiode under condition of the avalanche multiplication of carriers and the Franz–Keldysh effect.

We would like to thank E.Yu. Kolyadina for the help in ER measurements.

1. *Semiconductors and Semimetals* (Academic Press, New York, 1987), vol. 24.
2. Zh.I. Alferov, Semicond. **32**, 3 (1998).
3. V.V. Mitin., V.A. Kochelap, and M. Stroscio, *Quantum Heterostructures for Microelectronics and Optoelectronics* (Cambridge Univ. Press, Cambridge, 1999).
4. T.Ya. Gorbach and S.V. Svechnikov, Ukr. Fiz. Zh. **31**, 1110 (1987).
5. W. Lang, Mater. Sci. Eng. **R17**, 1 (1996).
6. E.F. Venger, T.Ya. Gorbach, L.A. Matveeva, and S.V. Svechnikov, Zh. Eksp. Teor. Fiz. **89**, 948 (1999).
7. T.Ya. Gorbach, P.S. Smertenko, S.V. Svechnikov, V.P. Bondarenko, R. Ciach, and M. Kuzma, Sol. Energy Mat. & Sol. Cells **72**, 529 (2002).
8. T.Ya. Gorbach, E.V. Pidlisnii, and S.V. Svechnikov, Optoelektr. Poluprov. Tekhn. **13**, 34 (1988).
9. R. Ciach, Yu.P. Dotsenko, V.V. Naumov, A.N. Shmyryeva, and P.S. Smertenko, Sol. Energy Mat. & Sol. Cells. **76**, 613 (2003).
10. A.Ya. Shik, Semiconductors **8**, 1841 (1974).
11. M. Cardona, *Modulation Spectroscopy* (Academic Press, New York, 1969).
12. G. Wisz, T.Ya. Gorbach, P.S. Smertenko, A. Blahut, K. Zembrowska, and M. Kuzma, Superlatt. Microstruct. **36**, 353 (2004).
13. G.E. Stillman and C.M. Wolfe, *Semiconductors and Semimetals* (Academic Press, London, 1977), Vol.12.

Received 11.07.06

ТРАНСПОРТ НОСІЇВ ЗАРЯДУ, СПЕКТРАЛЬНИЙ ФОТОВІДГУК ТА ОСОБЛИВОСТІ ЗОННОЇ СТРУКТУРИ В pnn^+-GaAs З НАНОРОЗМІРНИМ As_2O_3—GaAs ПАТЕРН-ІНТЕРФЕЙСОМ

Т.Я. Горбач, Л.А. Матвеєва, П.С. Смертенко, Г.О. Сукач

Р е з ю м е

З метою вивчення нових оптичних явищ і механізмів перенесення заряду досліджено поліпшені патерні структури As_2O_3—pnn^+-GaAs шляхом аналізу їх вольт-амперних характеристик (ВАХ), спектрального фотовідгуку (ФВ), зображень у скануючому електронному мікроскопі, а також методами рентгенівського аналізу та спектроскопії електровідбиття. Патерні напівпровідникові середовища розвинені одночасно з утворенням арсенолітової оксидної фази As_2O_3 за допомогою анізотропного хімічного травлення (АХТ) у (10–15)N розчині азотної кислоти HNO_3 верхньої поверхні p-типу структури pnn^+-GaAs. Було знайдено, що це середовище складається зі скелетно-дендритних морфологічних структур з розмірами приблизно 5–10 мкм, вкритих хемосорбованим нанорозмірним шаром As_2O_3 і нестехіометричними шарами з вакансіями Ga і вільним As на межі поділу As_2O_3—GaAs. Показано, що у сприятливих умовах для виникнення патерну біля поверхні утворюється інверсійний шар у вигляді ями із трикутним потенціалом і змінною шириною від 14 до 25 нм. У цьому випадку на темновій ВАХ у прямому напрямку спостерігається ділянка негативного диференціального опору з осциляційною поведінкою і відношенням струмів на вершині й у долині від 10 до 100, що є типовим для квантованої структури. Спектральні дані показали підвищення короткохвильової частини спектра відносно довгохвильової. Виявлено також вплив режиму виникнення патерну на фотовольтаїчні параметри. Для вищих значень зворотної напруги реалізовано підвищення коефіцієнта ФВ аж на 4 порядки завдяки лавинному розмноженню. Виявлення фотовідгуку поза нормальним краєм поглинання в GaAs може бути пояснено ефектом Франца–Келдиша. Запропоновано модель розвитку скелетно-дендритної багатошарової патерн-структури As_2O_3—pnn^+-GaAs під час АХТ. Обговорюються механізм переносу заряду й особливості структури забороненої зони.